

DIRECT NUMERICAL SIMULATION OF THE CHEMICALLY REACTING BOUNDARY LAYER OF HYPERSONIC FLOWS SUBJECT TO ABLATION

Mona Karimi & Christian Stemmer

Chair of Aerodynamics and Fluid Mechanics, Boltzmannstr.15
Technical University of Munich, 85748 Garching bei München, Germany

ABSTRACT

Extreme environment of the hypersonic regime of planetary entry flights prompts great challenges on the assessment of surface aeroheating and aerothermal prediction of the boundary layers over spacecrafts, leading to conservatism in design of the Thermal Protection System (TPS) of entry vehicles. Using ablative materials for the heat shield of TPS is the only viable choice to mitigate extreme heat fluxes of such high-enthalpy environments. To better model ablation process in the high-enthalpy hypersonic flow simulations, setting up the correct boundary conditions at the material surface is of paramount importance. We here investigate the role of the boundary condition on the surface aeroheating utilizing Direct Numerical Simulations (DNS) of the hypersonic flow over a flat plate subject to ablation. We also address how the extent of this investigation would differ in the cases of the significant out-gassing rates compared to that in the absence of out-gassing.

Index Terms— Hypersonic boundary layer, out-gassing, surface aeroheating

1. INTRODUCTION

Ablative materials are porous reactive materials containing several layers of solid phases and a single gas phase, imposing significant difficulties to determine the surface conditions of the boundary-layer flows of the ablative heat shield of the Thermal Protection Systems (TPS) of spacecraft. Modeling gas-surface interaction between the ablative material and boundary layer flow is one of the major issues in designing TPS. Ablation can affect the gas-surface interaction via three routes of (i) injecting pyrolysis gases and/or out-gassing of other ablation subproducts to the boundary layer, (ii) modifying the surface roughness due to the irregular pyrolysis, and (iii) altering the surface heat transfer due to the material-flow chemical reactions. The role of each route on the gas-surface interaction can vary depending on the trajectory of entry flight. The comparable effects of these three routes on the boundary-layer flow and consequently surface aeroheating have not been understood yet. Determining the heat transfer coefficient and thermal response of ablative materials to

high-enthalpy flows remains a challenge for the hypersonic vehicle design community.

Most experimental and numerical studies have focused on either the effect of ablation-induced blowing [1] or isolated effect of the surface roughness [2], while the combined effects on hypersonic boundary layer transition and surface heating are rarely taken into an account with the exception of few recent studies on porous coating and transpiring surfaces [3, 4]. There is a stark discrepancy between flight data and simulated heating rate of hypersonic flows over blunt bodies. A major uncertainty in simulating hypersonic boundary layers can be associated to the lack of understating of the driving mechanisms behind laminar-turbulent transition. Using laminar hypothesis to simulate the flow field results in disagreement with surface aeroheating rate measurements of hypersonic vehicles [5, 6]. On the other hand, fully turbulent simulations of hypersonic flows over blunt bodies over-predict the surface heat flux in the upstream regions [7, 8]. Most stability analyses of hypersonic boundary layer consider the idealized scenarios of homogeneous blowing and calorically perfect gas with no chemical reaction [9, 10, 11], while a recent review by Candler [12] shows that chemical reaction and vibrational energy can have an important effect on the instability growth leading to boundary-layer transition and surface heating. Empirical methods or engineering correlations are still being used as a set of practical tools to predict heat transfer rates and skin friction in high-speed flows. Among these correlations, in absence of a transition model, most designs of entry vehicles still follow some laminar solutions as a lower bound and turbulent correlations such as the van Driest's as an upper bound [13]. These correlations tend to over-predict heat transfer coefficients or Stanton number on cold walls ($T_w/T_\infty < 0.1$) and under-predict them otherwise. Over-prediction of nose surface recession of the ablative heat shield of the Galileo probe has been attributed to a high level of inaccuracy in calculating the thermochemical state of the flow field [14], and thus failure of the heating-ablating analysis tools [15]. The forebody of the Galileo probe is made of carbon-phenolic, a high-density material used in ablative heat shields under extreme conditions. Although pyrolysis-gas production can trigger transition in the laminar boundary-layer stagnation region [16], it is argued

that the injection-induced turbulence decays due to acceleration around the nose, and that convective heating is less important than radiative heating in the Galileo case [14]. While most numerical studies have focused on the isolated effect of each route on the surface aeroheating, we here aim to examine the combined effects of out-gassing as well as the material-flow chemical reaction on surface heating of the hypersonic boundary layer flow.

The objective of this work is to understand the underlying physical mechanisms of convective-blockage effects by ablation-induced blowing on the aeroheating of a hypersonic boundary-layer flow. Toward developing an engineering-level analysis tool to correlate the experimental data of heating with surface blowing, we need to obtain a sound level of fundamental understanding of the effects of mass transfer on aeroheating. As a first step of modeling gas-surface interactions on an ablative heat shield, we aim to scale the heat transfer coefficient with an appropriate blowing parameter in the absence of surface roughness. In §2 different parameterizations of blowing rate and injection-induced diffusivity are discussed while briefly introducing gas-surface interactions in the context of ablative TPS materials. The numerical framework along the boundary conditions and initialization are presented in §3, followed by results and discussion in §4 and finally we close by summary and future outlook in §5.

2. THEORETICAL BACKGROUND

2.1. Non-dimensionalization and scaling of blowing

Blowing or out-gassing rates can be characterized by a non-dimensional parameter differently depending on various parameters such as the geometry of the boundary layer or the shape of surface roughness, to name a few. Early experimental study of the laminar boundary-layer flow of certain binary gas mixtures [17] characterizes blowing or injection rate at the wall by a single non-dimensional parameter defined as:

$$F_w = \frac{\rho_w v_w}{\rho_\infty u_\infty}, \quad (1)$$

where ρ_w and v_w are density and normal velocity of the blown gas at the wall, respectively. Density and velocity of the inviscid freestream are denoted by ρ_∞ and u_∞ , respectively. With a minimal error, one can replace the freestream value in (1) with the mass flow rate per unit area at the boundary layer edge ($\rho_e u_e$), however at the cost of determining the correct location of the boundary layer edge. To include the non-uniform distribution of gas injection along the heatshield surface and the porosity of the surface, F_w can be modified by the base area of blowing and cross-sectional area of the porous section [18]. Since the distribution of blowing may not be uniform during pyrolysis, therefore the area-averaged blowing parameter can be modified as: $F_{w,a} = (\rho_\infty u_\infty A_{tot})^{-1} \int_0^{A_g} (\rho_w v_w) dA$, where A_{tot} is the total surface area of the boundary layer and A_g is surface areas that

pyrolysis gas is blown from. Such a scaling is more appropriate for flows over flat plates or blunt bodies at zero Angle of Attack (AOA), where classical inflection-point instability is the major player. While three-dimensional flows over the bodies at non-zero AOA can introduce an additional instability such as cross-flow instability [1].

To include the influence of blowing on aeroheating, film coefficient C_{H_o} of the non-blowing wall can be used to characterize a non-dimensional blowing parameter defined as [19]:

$$F_w^* = \frac{\rho_w v_w}{\rho_e u_e C_{H_o}}, \quad (2)$$

where $C_{H_o} = q_w / (\rho_e U_e C_p \Delta T)$ is the Stanton number for heat transfer or film coefficient of the non-blowing wall. Note that since F_w^* characterizes blowing locally as opposed to the averaged notion of $F_{w,a}$, it can give us the flexibility of investigating aeroheating of the stagnation-point region or any locations of interest that temperature or heat flux measurements are available. Then we can compare the aeroheating of these regions against the one of the same locations but with no blowing.

Finally, in some efforts of coupling between material response analysis and aerothermal calculation of the boundary layer, blowing can be scaled by the mass transfer coefficient, where C_{H_o} in Eq. (2) is replaced by C_M . That leads to a new non-dimensional parameter characterizing blowing rates at the wall defined as [20]:

$$B' = \frac{\dot{m}_{tot}}{\rho_e u_e C_M}, \quad (3)$$

where $\dot{m}_{tot} = \dot{m}_g + \dot{m}_{ca}$ is the mass-flow rate (per unit area) of the total injected gas in which the mass-flow rate of the pyrolysis gas and char ablation gas are denoted by \dot{m}_g and \dot{m}_{ca} , respectively. The Stanton number for mass transfer is denoted by $C_M = \dot{m}_s / [\rho_e u_e (c_{s_e} - c_{s_w})]$, where \dot{m}_s is the mass flow rate of species s . The mass fraction of species s at the boundary-layer edge and the wall are denoted by c_{s_e} and c_{s_w} , respectively. In the present study, we use the scaling notion of (2) to non-dimensionalize the velocity of gas blowing into the boundary layer to explicate the relationship between surface out-gassing and aeroheating in the hypersonic boundary layers.

2.2. Gas-surface interaction

To compute the aerothermal environment of the atmospheric entry flights, surface heat flux is inferred from the temperature measurements and thermal response assumptions, where the latter is either empirically modeled through calibration or explicitly modeled via a mathematical analysis. In this case, surface heating must be inferred from the actual sensor measurements of the embedded thermocouples inside the ablative heatshield of the TPS of a spacecraft. On an ablator, the location of boundary varies due to recession and chemical interac-

tions. The recession model is used to estimate this surface location. Considering the ablator as a solid material composite of multiple components and pyrolysis zone, surface temperature can be obtained by solving the energy transport equation from the perspective of the gas-surface interaction. By conducting the surface energy balance, the storage rate of sensible heat evaluated at a recessed coordinate (y_r) is given by:

$$\rho c_p \frac{\partial T}{\partial t} \Big|_{y_r} = \frac{1}{A_{tot}} \frac{\partial}{\partial y_r} \left(k A_{tot} \frac{\partial T}{\partial y_r} - q_{rad} \right) + \frac{\dot{m}_g}{A_g} \frac{\partial h_g}{\partial y_r} + (h_g - \bar{h}) \frac{\partial \rho}{\partial t} \Big|_y + \dot{s} \rho c_p \frac{\partial T}{\partial y_r} \quad (4)$$

where y is the stationary coordinate system in which the virgin material resides initially and y_r is the coordinate system moving with the recession surface. The local cross-section of the material exposed to the pyrolysis gas mass-flow rate (\dot{m}_g) and enthalpy (h_g) is denoted by A_g that is heated via conduction and pyrolysis gas convection. The surface recession rate is denoted by \dot{s} , enthalpy by h and temperature by T . We here assume that partially pyrolyzed material is a simple mixture of pure virgin material and pure char. Therefore density of the partially pyrolyzed material is denoted by ρ such that $\rho_c < \rho < \rho_v$, where the virgin and char material properties are denoted by $(\cdot)_v$ and $(\cdot)_c$, respectively. The mass fraction of the virgin material in a mixture of virgin material and char denoted by r_v is defined by $r_v = (1 - \frac{\rho_c}{\rho}) / (1 - \frac{\rho_c}{\rho_v})$. Similar to density, all other material properties of a mixture used in Eq. (4) such as specific heat coefficient (c_p) and thermal conductivity (k) are weighted following the mixture rule, $(\cdot) = (\cdot)_v (\cdot)_{p,v} + (1 - r_v) (\cdot)_{p,c}$.

As the material is heated, one (or more) component(s) of virgin material pyrolyzes and produces char and pyrolysis gas, yielding out-gassing or injecting mass which percolates away from the pyrolysis zone and goes through pores of charred zone and finds its way to the boundary-layer flow. Besides injecting mass, there is also heat flux into the boundary layer. The first term on the RHS of Eq. (4) is the net rate of conductive and radiative heat flux. The second term on the RHS is the rate of energy convected by pyrolysis gas, the third term is consumption rate of the pyrolysis energy, and finally the last term on the RHS of the Eq. (4) is rate of convective (sensible) heat flux due to recession. The quantity \bar{h} in Eq. (4) is the density weighted enthalpy difference between the virgin material and char defined by $\bar{h} = \frac{\rho_v h_v - \rho_c h_c}{\rho_v - \rho_c}$. The enthalpy of the pyrolysis gas is a function of the wall temperature, pressure and mass fraction: $h_g = f(T_w, p_w, r_v)$ [21].

2.3. Boundary conditions

To consider the ablation process in the high-enthalpy hypersonic flow simulation, surface boundary conditions are tremendously more complicated than modeling the passive material or the more conventionally used no-slip boundary conditions. Here we assume a non-catalytic surface. The computational domain along the boundary conditions are

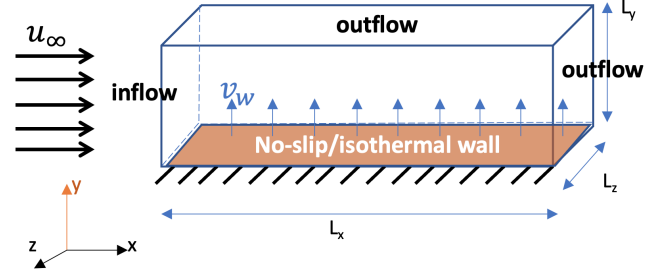


Fig. 1. Sketch of the DNS domain with boundary conditions.

shown in Figure 1. Blowing or out-gassing boundary condition at the bottom wall is implemented by altering the normal component of velocity at the surface as schematically depicted in Figure 1. Ablative materials are porous reactive materials containing several layers of solid phases and a single gas phase. Modeling mass and heat transfer from such materials to the boundary layers requires a coupling strategy incorporating the ablating surface energy balance and the aerothermal environment calculations. The main idea here is to solve the compressible Navier-Stokes equations, along with the continuity of each species, and the two-temperature model of energy transport equations. However to model the energy balance at the gas-surface interface, we need to calculate the heating influx from the environment into the boundary layer and cooling out-flux from the effective surface of the porous material to the boundary layer as illustrated in literature [22]. Therefore, it is necessary to locate the boundary-layer edge and to calculate boundary-layer parameters in a separate step.

The bottom wall (orange surface in Figure 1) is assumed to be an isothermal wall boundary condition on temperature and no-slip on velocity. The constant cold temperature is $T_w/T_e = 6.5$ close to the laminar adiabatic wall temperature or about 79 % of the stagnation temperature, where T_w and T_e are temperature at the wall and boundary layer edge, respectively. In the spanwise (z) direction, periodic boundary conditions are used whereas characteristic outflow boundary conditions are used on the top and downstream boundaries.

3. NUMERICAL METHOD

To compute the flowfield, we use an open-source code, the Hypersonics Task-based Research (HTR) solver [23] developed for DNS of hypersonic flows subject to aerothermochemical effects in structured grids, while including the finite-rate chemistry and thermal non-equilibrium. In order to handle the stiffness induced by vastly different time scales with efficiency and stability, the solver here employs two different time-advancement schemes: a third-order Runge-Kutta method when the chemical reactions are slow, and an operator-splitting method when chemical reactions are fast and the numerical integration becomes correspondingly

stiff. For spatial discretization, a low-dissipation sixth-order targeted essentially non-oscillatory (TENO) scheme is used as a compromise solution between low numerical dissipation and stable capture of shocks. The viscous terms are computed with second-order spatial accuracy with a central difference approach. Since the HTR solver is based on a multi-component transport formulation, we can incorporate variable specific heat capacities and transport coefficients along with a chemical-kinetic description for air dissociation. This formulation enables the investigation of phenomena induced by vibrational excitation of air molecules and their dissociation in hypersonic flows at high Reynolds numbers.

To accurately represent the high-enthalpy flows, modeling the gas transport properties is crucial. Here, the diffusion coefficients of the multi-component of the gas mixture are evaluated using the self-consistent effective binary diffusion model [24]. The mixture viscosity and thermal conductivity of multi-species gas are evaluated by using the kinetic-theory-based model and Yos approximate mixing rules [25]. To compute vibrational thermal conductivity, the standard expression with vibrational temperature gradients is used as since simulations with energy gradients tend to be unstable for the dissociated flow. The advantage of the HTR solver is in deployment of the GPU-based high-performance computation. In contrast to the traditional domain-decomposition methods in the parallel CFD solvers, the HTR solver is developed on the task-based environment provided by the versatile libraries of the programming language model of Legion [26]. Specifically designed for writing memory-hierarchy-agnostic programs, Legion is more efficient and less costly in memory-management operations compared to the conventional Message Passing Interface (MPI) structures.

For all simulations, the Reynolds number is based on inflow displacement thickness and freestream viscosity and freestream velocity: $Re = \delta_0^* \rho_\infty u_\infty / \mu_\infty = 3000$, where μ_∞ is dynamic viscosity and ρ_∞ density of freestream, δ_0^* is the displacement thickness of the boundary layer at the inflow boundary condition located at $x = x_0$. This is the start of an undisturbed compressible laminar boundary layer, in which velocity and temperature profiles are imposed by self-similar solutions. Note that the origin of the streamwise coordinate $x = 0$ corresponds to the leading edge of the plate, which is not considered as $x = x_0$ in these calculations. The power law $\mu = \mu_{\text{ref}} (T/T_{\text{ref}})^\sigma$ is used to compute dynamic viscosity of the gas, where with $\sigma = 0.7$, and where μ_{ref} is a reference value of viscosity evaluated at the reference temperature T_{ref} . Once c_p and μ are calculated, the thermal conductivity in Eq. 4 $k = Pr/\mu c_p$ is evaluated by assuming a constant value of the Prandtl number, Pr .

All lengths in the computational domain schematically shown in Figure 1 are non-dimensionalized by δ_0^* for the simulation. The domain is rectangular with uniform spacing in the spanwise (z) and streamwise (x) directions whereas a hyperbolic-tangent stretching is used in the wall-normal (y)

direction in order to cluster cells near the wall. The stretching parameter of the distribution is determined by enforcing that the wall-normal size of the first grid element close to the wall. Therefore $\Delta y^+ = 0.3$ which is normalized in viscous units measured at the exit domain boundary, while in the streamwise and spanwise directions are $\Delta x^+ = 2.0$ and $\Delta z^+ = 1.8$, respectively. A summary of the domain size, number of grid points and resolution for all simulation scenarios can be found in Table 1.

Table 1. Summary of DNS computation setup with $Re_{\theta, max} = 2650$, $M = 6$ and $T_w/T_e = 6.5$

N_x	N_y	N_z	L_x	L_y	L_z	Forcing amplitude
4096	250	288	1000	75	20π	$0.05U_e$

The distribution of the out-gassing velocity v_w is assumed to be uniform with the form of

$$v_w = f(x) \sum_i^2 A_i \sin(\omega_i t - \beta_i z) \quad (5)$$

where $f(x) = \frac{1}{4x_s} \left[\text{erf} \left(\frac{x+x_s}{\sigma\sqrt{2}} \right) - \text{erf} \left(\frac{x-x_s}{\sigma\sqrt{2}} \right) \right]$

where the function $f(x)$ forces a Gaussian-like profile of perturbation in the streamwise (x) direction, with $x_s = 15\delta_0^*$ and $\sigma = 0.75\delta_0^*$ and δ_0^* is the boundary layer displacement thickness at the inflow boundary condition. To achieve the oblique breakdown, we use two opposite modes parametrized by the wavemode amplitude of $A = [0.05u_\infty, 0.05u_\infty]$, the wavemode frequency of $\omega = [0.9\delta_0^*/a_\infty, 0.9\delta_0^*/a_\infty]$, and the spanwise wavenumber of $\beta = [0.3/\delta_0^*, -0.3/\delta_0^*]$, where a_∞ is speed of sound in the freestream. Freestream velocity u_∞ can be evaluated based on the freestream Mach number $M_\infty = 6$ and $T_\infty = 450$ K.

4. RESULTS

Skin friction of the laminar boundary layer over the non-blowing surface is contrasted against boundary layer over the surface with the blowing parameter of $F_w = 0.005$, depicted in Figure 2.

Comparing the case of the boundary layer over the non-blowing wall with the one for the blowing case (solid lines in Figure 2), we observe the slight increase in skin friction defined as $C_f = \tau_w / (1/2\rho_\infty u_\infty^2)$, where τ_w is the wall shear stress. Surface blowing introduces more mass momentum to the boundary layer, results in the increase of viscous force. However, the heat transfer per unit area q_w shown in Figure 2 (dashed lines) is inhibited by the surface blowing. This is the verification of what has been hypothesized earlier that injecting pyrolysis gas into the boundary layer reduces the heat transfer rate via *convective blockage effect* [27].

The effect of out-gassing on the local characteristics of a boundary layer is examined in terms of the spanwise vortic-

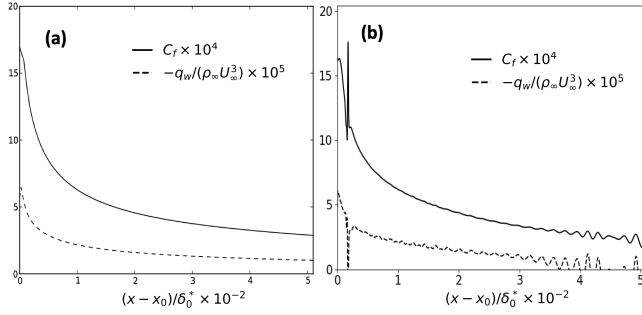


Fig. 2. Spanwise- and time-averaged skin-friction coefficient, C_f and normalized heat-flux, $q_w / \rho_\infty u_\infty^3$ at the wall as function of the normalized streamwise coordinate $(x - x_0) / \delta_0^*$ for (a) the non-blowing case $F_w=0$ and (b) the case of out-gassing rate of $F_w=0.005$.

ity for three blowing rates as shown in Figure 3. Except the growth of the boundary layer thickness, it seems that vorticity structures remain intact but that is not the cases as more gas is blown into the boundary layer. This is also evident from the density contour plots in Figure 4. Also the laminar structure of the flow is disturbed as blowing rate increases (as shown Figure 4 (c), presumably the flow is triggered toward more transition regime, though not being achieved yet.

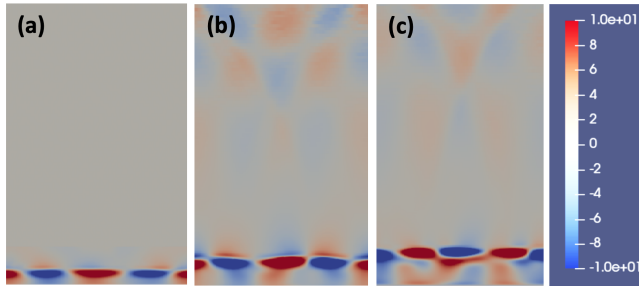


Fig. 3. Contour plots of vorticity for (a) the non-blowing case $F_w=0$, (b) the case of out-gassing rate of $F_w=0.005$ and (c) 0.01. For all three scenarios the vorticity at the distance of $0.75L_x$ from the leading edge of the boundary layer is plotted.

Since the present simulations utilize a numerical method that does not use any filter nor requires any flux limiter, higher resolution across the boundary layer especially in the stream-wise and normal directions has been implemented. Here, the blown gas has the same temperature as the surface temperature, therefore the pyrolysis gas enthalpy h_g in Eq. (4) is not accurately modelled yet. Also the injection gas has the same composition as the freestream gas, a binary air mixture of 79% N_2 and 21% O_2 , which is in in chemical equilibrium at temperature $T_\infty = 450$ K and pressure $P_\infty = 1$ atm. The chemical equilibrium in the freestream is largely displaced toward the reactants and leads to a negligible dissociation degree. Zero wall-normal gradients are imposed for all species mass

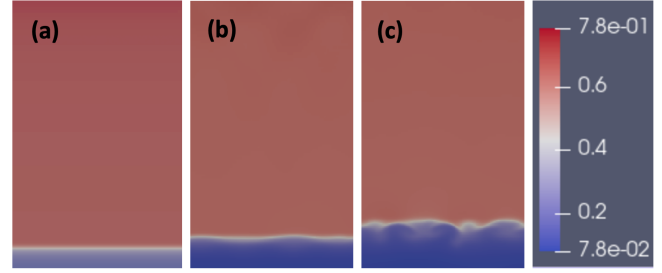


Fig. 4. Contour plots of density for (a) the non-blowing case, (b) the case of out-gassing of F_w 0.005 and (c) 0.01 at $0.75L_x$.

fractions at the wall. The inflow boundary conditions are obtained by solving the laminar, locally self-similar boundary-layer equations including species transport and chemical reactions. The more interesting question is how the results alter in case of injecting a foreign gas, also at the temperature that corresponds to the material response modeling the ablative material behavior at the surface.

5. CONCLUSION

Ablation manifested by mass injection pushes the laminar boundary-layer edge away from the surface and shields the body from the high-temperature shock-layer gas. The response of the laminar boundary layer to surface blowing is an augmentation of density due to additional mass transfer and the reduction of viscosity at the wall which is primarily attributed to the cooling effect of surface blowing. Out-gassing has a minimal effect on the wall pressure in laminar boundary layers. To reduce uncertainty in calculation of the hypersonic boundary-layer flow field as well as to expand on the investigation of the effect of mass transfer on aerothermal heating, more sensitivity analyses implementing the local or point-wise injection velocity at the wall and also more computationally-demanding variations of in-depth properties are needed. Depending on which ablative material is used, the type and concentration of pyrolysis gas mixture vary. To provide a deeper understating of the physical mechanism underlying the effect of out-gassing on aerothermal flow field, we indeed demand more experimental data in high-enthalpy boundary flows. This work is one step toward understanding the fluid-structure interaction via blowing effect on aeroheating at the extreme environment of hypersonic flight, though realizing high-fidelity simulations of the hypersonic flow environment is far from complete. Since hypersonic flight systems undergo various changes during flight over a large range of time scales, it is important to include relevant processes such as roughness modification, material degradation, shape change, and recession.

6. ACKNOWLEDGMENTS

The authors gratefully acknowledge the computing time granted through Gauss Centre Supercomputing Program on the supercomputer JUWELS Booster and Cluster partitions at Forschungszentrum Jülich. The first Author is grateful to the generous support of the Laura-Bassi fellowship provided by the government of the state of Bavaria and hosted by the Technical University of Munich.

7. REFERENCES

- [1] S. P. Schneider, "Hypersonic boundary-layer transition with ablation and blowing," *J. Spacecr. Rockets*, vol. 47, pp. 225–237, 2010.
- [2] D. Reda, W. Wilder, D. Bogdonoff, and D. Prabhu, "Transition experiments on blunt bodies with distributed roughness in hypersonic free flight," *J. Spacecr. Rockets*, vol. 45, no. 2, 1970.
- [3] S. A. Gaponov, Y. G. Ermoleaev, A. D. Kosinov, V. I. Lysenko, N. V. Semenov, and B. V. Smorodskii, "Influence of porous-coating thickness on the stability and transition of flat-plate supersonic boundary layer," *Thermophysics and Aeromechanics*, vol. 19, no. 4, pp. 555–560, 2012.
- [4] J. Meinert, J. Huhn, E. Serbest, and O.J. Haidn, "Turbulent boundary layers with foreign gas transpiration," *J. Spacecr. Rockets*, vol. 38, no. 2, pp. 191–198, 2001.
- [5] B.R. Hollis and J.N. Perkins, "Transition effects on heating in the wake of a blunt body," *J. Spacecraft Rockets*, vol. 36, pp. 668–674, 1999.
- [6] Z.X. Gao, H.C. Xue Xue, Z.C. Zhang, H.P. Liu Liu, and C.H. Lee, "A hybrid numerical scheme for aero-heating computation of hypersonic reentry vehicles," *Intl. J. Heat Mass Transfer*, vol. 116, pp. 432–444, 2018.
- [7] S.J. Ju, C Yan, X.Y. Wang, Y.P. Qin Qin, and Z.F. Ye, "Sensitivity analysis of geometric parameters upon the aerothermodynamics of mars entry vehicle," *Intl. J. Heat Mass Transfer*, vol. 120, pp. 597–607, 2018.
- [8] Z. Xiao, G. Wang, M. Yang, and L. Chen, "Numerical investigations of hypersonic transition and massive separation past orion capsule by DDES-TR," *Intl. J. Heat Mass Transfer*, vol. 137, pp. 90–107, 2019.
- [9] F. Li, M. Choudhari, C.L. Chang, and J. White, "Effects of injection on the instability of boundary layers over hypersonic configurations," *Phys. Fluids*, vol. 25, no. 104107, pp. 1–15, 2013.
- [10] S. Ghaffari, O. Marxen, G. Iaccarino, and E. Shaqfeh, "Numerical simulations of hypersonic boundary-layer instability with wall blowing," *AIAA Paper no.2010-0706*.
- [11] C. H. Mortensen and X. Zhong, "Real-gas and surface-ablation effects on hypersonic boundary-layer instability over a blunt cone," *AIAA Journal*, vol. 54, no. 3, pp. 976–994, 2016.
- [12] G. V. Candler, "Rate effects in hypersonic flows," *Annu. Rev. Fluid Mech.*, vol. 51, pp. 379–402, 2019.
- [13] E. R. van Driest, "On turbulent flow near a wall," *J. Aeronaut. Sci.*, vol. 23, pp. 1007–1011, 1956.
- [14] S. Matsuyama, N. Ohnishi, A. Sasoh, and K. Sawada, "Numerical simulation of galileo probe entry flowfield with radiation and ablation," *Journal of Thermophysics and Heat Transfer*, vol. 19, no. 1, pp. 28–35, 2005.
- [15] C. Park, "Stagnation-region heating environment of the galileo probe," *Journal of Thermophysics and Heat Transfer*, vol. 23, no. 3, pp. 417–424, 2009.
- [16] C. Park, "Injection-induced turbulence in stagnation-point boundary layers," *AIAA Journal*, vol. 22, no. 2, pp. 219–225, 1984.
- [17] C. C. Pappas and A. Okuno, "Heat-transfer measurement for binary gas laminar boundary layers with high rates of injection," *NASA TN-D-2473*, 1964.
- [18] F. Miró Miró, P. Dehairs, F. Pinna, M. Gkolia, D. Masutti, T. Regert, and O. Chazot, "Effect of wall blowing on hypersonic boundary-layer transition," *AIAA Journal*, vol. 57, no. 4, 2019.
- [19] W. H. Dorrance, *Nonequilibrium Hypersonic Aerothermodynamics*, Dover Publications, New York, 2017.
- [20] Y. K. Chen and F. S. Milos, "Ablation and thermal response program for spacecraft heathshield analysis," *J. Spacecr. Rockets*, vol. 36, no. 3, pp. 475–483, 1999.
- [21] G. Duffa, *Ablative Thermal Protection System Modeling*, AIAA Education Series, 2013.
- [22] J Lachaud, T. van Eekelen, J.B. Scoggins, T.E. Margin, and N.N. Mansour, "Detailed chemical equilibrium model for porous ablative materials," *Intl. J. Heat Mass Transfer*, vol. 90, pp. 1034–1045, 2015.
- [23] M. Di Renzo, L. Fu, and J. Urzay, "HTR solver: An open-source exascale-oriented task-based multi-GPU high-order code for hypersonic aerothermodynamics," *Comp. Physics Comm.*, vol. 255, no. 107262, 2020.

- [24] J.D. Ramshaw and C.H. Chang, "Ambipolar diffusion in two-temperature multicomponent plasmas," *Plasma Process*, vol. 13, no. 3, pp. 489–98, 1993.
- [25] R. Gupta, J. M. Yos, R. Thompson, and K Lee, "A review of reaction rates and thermodynamic and transport properties for an 11-species air model for chemical and thermal nonequilibrium calculations to 30000 k," 1990.
- [26] "<https://legion.stanford.edu/publications/>," .
- [27] C. Park, "Hypersonic aerothermodynamics: Past, present and future," *Int'l. J. of Aeronautical & Space Sci.*, vol. 14, no. 1, pp. 1–10, 2013.